Complexity evaluation of MOMA: We observe that the proposed structure consists of a CSA tree, which requires $D = \lceil \log_2 p/(\log_2 3-1) \rceil$ node levels, and a final adder/converter block. The CSA tree has $< \lceil p/3 \rceil D/2$ nodes (i.e. the area of the triangle containing the tree). Each node consists of two CSAs of n bits and of an $8\times n$ multiplexer. The final MAC has three CSAs and four carry look-ahead adders (CLA) of $n+3$ bits at most and an $8\times n$ multiplexer. The response time is

$$T_A = \left\lceil \frac{\log_2 p - 1}{\log_2 3 - 1} \right\rceil (2t_{CSA} + t_{MUX(8\times n)}) + t_{CSA} + t_{CLA(n+3)} + t_{MUX(8\times n)} \quad (1)$$

Recalling that $t_{CLA(h)} = 2+4\lceil \log 4h \rceil$ gate delays Δg for operands of h bits [6], T_A is $\vartheta(\log_2 p+\log_2\log_2 m)$ and appears to be more attractive than results in the literature [1 – 3].

Application to the generation of $|X|_m$: It is well known that, given a positive integer $X = \Sigma x_i 2^i \leq 2^r-1$, $x_i \in \{0,1\}$, the value of $|X|_m$ can be obtained as

$$|X|_m = \left| \sum_{i=0}^{r-1} x_i |2^i|_m \right|_m$$

This computation can be easily performed using a multioperand modular adder, whose inputs consist of terms $x_i \cdot |2^i|_m$. Note that each of these terms can be yielded by $\lceil \log_2 m \rceil$ AND gates between x_i and the bits of $|2^i|_m$. Therefore $|X|_m$ can be evaluated by means of a multioperand modular adder as in Fig. 2, with r inputs, each n bits wide.

As far as response time T_{Conv} is concerned, it can be derived from eqn. 1 replacing p by the length r of X and giving h the value $\lceil \log_2 m \rceil + 3$ (Fig. 3), i.e.

$$T_{Conv} = \left\lceil \frac{\log_2 r - 1}{\log_2 3 - 1} \right\rceil (2 \times t_{CSA} + t_{MUX(8\times n)}) + t_{CSA} + (4\lceil \log_4(\lceil \log_2 m \rceil + 3) \rceil + t_{MUX(8\times n)}) \quad (2)$$

To evaluate the performance of this conversion approach in a specific case, we choose the value $r = 128$ and observe from Fig. 1 that $t_{CSA} = 6\Delta g$ and $t_{MUX(8\times n)} = 2\Delta g$; then eqn. 2 becomes

$$\begin{aligned} T_{conv} &= \left\lceil \frac{\log_2 128 - 1}{\log_2 3 - 1} \right\rceil (2 \times 6 + 2) + 6 + 2 + 4\lceil \log_4(\lceil \log_2 m \rceil + 3) \rceil + 2 \\ &\simeq \frac{6}{0.58} \times 14 + 10 + 4\lceil \log_4(\lceil \log_2 m \rceil + 3) \rceil \\ &\simeq 155 + 4\lceil \log_4(\lceil \log_2 m \rceil + 3) \rceil \end{aligned}$$

Considering the worst case $m = 2^{128}-1$, it results that $T_{Conv} \simeq 155+4\times 4 = 171\ \Delta g$. In terms of complexity, $m = O(2^r)$ and therefore $T_{Conv} = \vartheta(\log_2 r)$.

24 October 1995
Electronics Letters Online No: 19960026

G. Alia (*Dipartimento di Ingegneria dell'Informazione, Università di Pisa, Via Diotisalvi 2, 56126 Pisa, Italy*)

E. Martinelli (*Dipartimento di Ingegneria Elettrica ed Elettronica, Università di Cagliari, Piazza d'Armi, 09123 Cagliari, Italy*)

References

1 SKAVANTZOS, L.: 'Design of multi-operand carry-save adders for arithmetic modulo (2^n+1)', *Electron. Lett.*, 1989, **25**, (17), pp. 1152–1153

2 KOÇ, C.K., and HUNG, C.Y.: 'Multioperand modula addition using carry save adders', *Electron. Lett.*, 1990, **26**, (6), pp. 361–363

3 PIESTRAK, S.J.: 'Design of residue generators and multioperand modular adders using carry-save adders', *IEEE Trans.*, 1994, **C-423**, (1), pp. 69–77

4 SZABO, N.S., and TANAKA, R.J.: 'Residue arithmetic and its applications to computer technology' (McGraw-Hill, New York, 1967)

5 ALIA, G., and MARTINELLI, E.: 'A VLSI structure for X (mod n) operations', *VLSI Signal Process.*, 1990, **1**, pp. 257–264

6 SCOTT, N.R.: 'Computer number systems and arithmetic' (Prentice-Hall International Editions, Englewood Cliffs, NJ, 1985)

Integral formulation of the measured equation of invariance

J.M. Rius

Indexing terms: Electromagnetic wave scattering, Finite difference methods, Integral equations

A novel integral formulation of the measured equation of invariance is derived from the reciprocity theorem. This formulation leads to a sparse matrix equation for the induced surface current, resulting in great CPU time and memory savings over the conventional approaches. The algorithm has been implemented for two-dimensional perfectly conducting scatterers.

Introduction: Recently, the measured equation of invariance (MEI) method has been introduced by Mei *et al.* [1] as a mesh truncation condition for the finite difference method. A later paper [2] analyses some theoretical and numerical aspects of the MEI. In this Letter we present the new concept of the MEI as a surface integral equation method derived from the reciprocity theorem, which produces a sparse matrix with the same number of unknowns as the conventional boundary element - method of moments (BE-MoM) technique. This new formulation has an important advantage over the original finite difference formulation: it requires a boundary discretisation instead of a volume discretisation, while maintaining the sparsity of the matrix.

Derivation from the reciprocity theorem: Let C be the boundary of a perfectly conducting (PEC) scatterer and C_n a portion of this boundary. Introduce two sets of electric and magnetic sources as follows:

1. The induced currents on the surface of the PEC scatterer $\vec{J}_s = \hat{n} \times \vec{H}|_C$ and $\vec{M}_s = -\hat{n} \times \vec{E}|_C = 0$, where $\vec{E}$ and $\vec{H}$ are the electric and magnetic fields actually existing in the presence of the scatterer. According to the equivalence theorem [4], this set of sources radiates the scattered fields in $\vec{E}^s = \vec{E} - \vec{E}^i$, $\vec{H}^s = \vec{H} - \vec{H}^i$ free space where $\vec{E}^i$ and $\vec{H}^i$ are the fields in the absence of the scatterer, or the incident fields.
2. A set $(\vec{J}_n, \vec{M}_n)$ that exists only over C_n and radiate fields $\vec{E}_n$, $\vec{H}_n$.

With these sets of sources, the reciprocity theorem [4] for a linear and isotropic medium is

$$\int_{C_n} \left(\vec{E}_t^s \cdot \vec{J}_n - \vec{H}_t^s \cdot \vec{M}_n \right) dl = \int_C \vec{E}_n \cdot \vec{J}_s \, dl \quad (1)$$

where $\vec{E}_t^s$ and $\vec{H}_t^s$, the components of the scattered fields tangential to the scatterer boundary, account for the fact that $\vec{J}_n$ and $\vec{M}_n$ represent surface currents. eqn. 1 is the integral equation formulation of the MEI (IE-MEI).

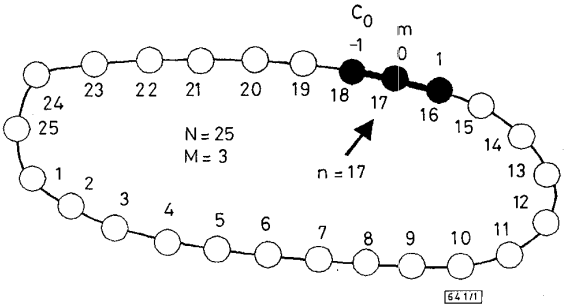

Fig. 1 *Boundary meshing of scatterer for IE-MEI*

For simplicity, only the discretisation for 2-D problems will be presented. The boundary C and its portion C_n are discretised into N and M segments of equal length h, respectively. Let C_n be centred at node n of C Fig. 1. The currents $\vec{J}_n$ and $\vec{M}_n$ are expanded along C_n into M pulse basis functions. If we define $\vec{a}_{n,n\oplus m} = h\vec{J}_n$ $(l_{n\oplus m})$ and $\vec{b}_{n,n\oplus m} = h\vec{M}_n$ $(l_{n\oplus m})$, we obtain

$$\sum_{m=-\frac{M-1}{2}}^{m=\frac{M-1}{2}} \left[\vec{a}_{n,n\oplus m} \cdot \vec{E}_t^s(l_{n\oplus m}) - \vec{b}_{n,n\oplus m} \cdot \vec{H}_t^s(l_{n\oplus m})\right] = \int_C \vec{E}_n \cdot \vec{J}_s \, dl \quad (2)$$

which is the discrete version of the IE-MEI. The addition of subscript indices is modulo N, so $n \oplus m$ assumes values from 0 to $N-1$.

The right-hand term in eqn. 2 is the residual $R_n = \int_C \vec{E}_n \cdot \vec{J}_s \, dl$. This residual has previously been obtained in [2] for the finite difference MEI using a different procedure. The $\vec{E}_n$ field corresponds to the 'null field' $\vec{E}_{null}$ of [2]. In our experience, the residual R_n can be made arbitrarily small for convex scatterer shapes with appropriate $\vec{a}_{n,n\oplus m}$ and $\vec{b}_{n,n\oplus m}$ coefficients.

Assuming that R_n is zero, in two dimensions we have

$$\sum_{m=-\frac{M-1}{2}}^{m=\frac{M-1}{2}} [a_{n,n\oplus m} E_t^s(l_{n\oplus m}) - b_{n,n\oplus m} H_t^s(l_{n\oplus m})] = 0 \quad (3)$$

where for TM polarisation $a_{n,n\oplus m} = -\vec{a}_{n,n\oplus m} \cdot \hat{z}$, $\vec{E}_t^s = -E_t^s \hat{z}$, $b_{n,n\oplus m} = \vec{b}_{n,n\oplus m} \cdot \hat{l}$, $\vec{H}_t^s = H_t^s \hat{l}$, for TE polarisation $a_{n,n\oplus m} = \vec{a}_{n,n\oplus m} \cdot \hat{l}$, $\vec{E}_t^s = E_t^s \hat{l}$, $b_{n,n\oplus m} = \vec{b}_{n,n\oplus m} \cdot \hat{z}$, $\vec{H}_t^s = H_t^s \hat{z}$ and $\hat{l}$ is the unit vector tangential to the scatterer boundary C.

To compute the coefficients $a_{n,n\oplus m}$ and $b_{n,n\oplus m}$ we use the same procedure as in the finite difference formulation of the MEI [1]: if in eqn. 2 the $\vec{E}_n$ function is orthogonal to the induced current $\vec{J}_s$, the residual is zero for all possible incident fields (the postulate of invariance of the MEI [1]). This fact suggests that if we know $P \geq 2M-1$ linearly independent scattered field solutions (called 'measuring functions') owing to P different incident fields, forcing eqn. 3 for each mesh node n we can obtain a set of $a_{n,n\oplus m}$ and $b_{n,n\oplus m}$ coefficients. This set of coefficients will also satisfy eqn. 3 with the actual scattered field. The measuring functions are obtained as the field radiated by a set of functions $\sigma_p(\vec{r}')$ defined on the scatterer boundary C, called 'metrons'.

Eqn. 3, which previously appeared in a conference presentation [3], is a linear relation between the tangential components of the electric and magnetic fields at M consecutive nodes in the portion C_n of the scatterer boundary centred at node n, where $n = 0 \ldots N-1$. This relation can be expressed more concisely as

$$[A][E_t^s] - [B][H_t^s] = 0 \quad (4)$$

where $a_{n,n\oplus m}$ are the elements of global matrix $[A]$, $b_{n,n\oplus m}$ are the elements of global matrix $[B]$ and $E_t^s(l_{n\oplus m})$, $H_t^s(l_{n\oplus m})$ are the components of vectors $[E_t^s]$ and $[H_t^s]$, respectively. The matrices $[A]$ and $[B]$ are cyclic band diagonal with bandwidth M.

Since the tangential component of the electric scattered field is known along the object boundary, $[E_t^s] = -[E_t^i]$, we can obtain the electric induced current as

$$[J_s] = [H_t^i] + [H_t^s] = [H_t^i] - [B]^{-1}[A][E_t^i] \quad (5)$$

Numerical considerations: The following set of metrons has been used to obtain the results presented in this Letter:

$$\sigma_p(l') = e^{-j2\pi p l'/L} \qquad |p| \leq \frac{P-1}{2}$$
$$P = 2kR_{max}\chi + 1 \qquad 0 \leq l' \leq L \quad (6)$$

These are harmonic functions along the scatterer boundary C to the order $P = kR_{max}\chi$, where R_{max} is the radius of the smallest cylinder enclosing the scatterer and χ is a coefficient slightly larger than one. Typical values of χ range from 1.05 to 1.30. In our experience, this set of metrons guarantees a small residual for two-dimensional problems when the PEC scatterer is a convex cylinder.

With regard to the number of nodes M in the linear relation eqn. 3, the best results are obtained with $M \geq 5$, although the best trade-off between computation time and accuracy is achieved with $M = 3$.

The memory requirement of our implementation of the IE-MEI in MATLAB 4.2 language is ~9.5 N complex numbers for a linear relation involving $M = 3$ boundary nodes. This means that for each megabyte of available memory the IE-MEI method can allocate 6900 unknowns.

For each unknown at the mesh truncation boundary, the number of operations is in principle proportional to P times the number of integration points at the boundary, Q. In our case, $Q = N$. However, it is noted that the field, owing to the metrons, as in eqn. 6 is a Fourier transform. For example, the electric field in the TM case is

$$E_p(\vec{\rho}_m) = -\frac{k\eta}{4} \int_0^L e^{-j2\pi p l'/L} H_0^{(2)}(k|\vec{\rho}_m - \vec{\rho}'|) dl' \quad (7)$$

and similar relations exists for the TM magnetic field and for the TE case. Therefore, if the boundary samples are equally spaced, the FFT algorithm can be used and the total number of operations is proportional to $NQ \log_2 Q$. In that case, it grows with frequency as $f^2 \log_2 f$.

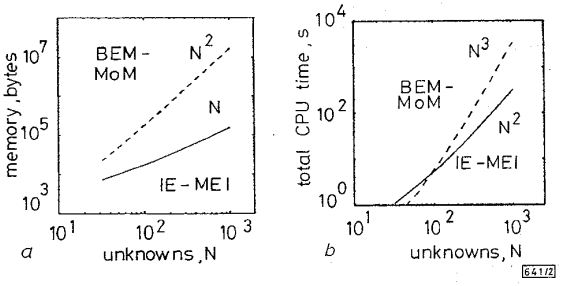

Fig. 2 *Computer memory*

a With CPU time
b Required by IE-MEI compared to BEM-MoM

Fig. 2 shows the computer memory and CPU time required by the IE-MEI method compared with method of moments (MoM). For an honest comparison, the same discretisation and computer code has been used in both methods for computing the radiation operators.

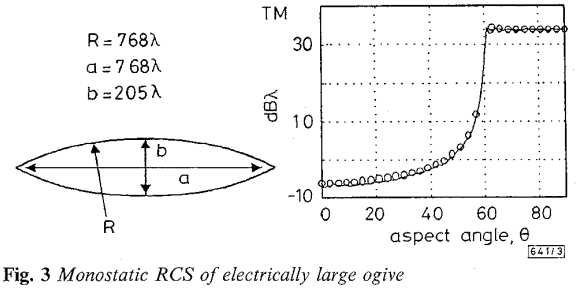

Fig. 3 *Monostatic RCS of electrically large ogive*

IE-MEI results are compared to GO + GTD high-frequency methods
O GO + GTD
——— MEI M = 3

Results: Fig. 3 shows the monostatic RCS of an ogival cylinder of dimensions 768λ × 205λ and perimeter 1620λ. This result was computed in a 486 DX-66 PC using only 2.3 MB of memory. The results of the IE-MEI are compared to high frequency approximations: geometrical optics (GO) and geometrical theory of diffraction (GTD). The agreement is excellent.

Acknowledgments: The author is indebted to Prof. K. Michalski of Texas A&M University for the valuable discussions on the MEI method. This work has been supported by the Spanish 'Comisión Interministerial de Ciencia y Tecnología' (CICYT) under project TIC 93-0518.

25 August 1995
Electronics Letters Online No: 19960028

J.M. Rius (*Department of DSC, Universitat Politècnica de Catalunya, Gran Capitán s/n, edifici D-3, 08034 Barcelona, Spain*)

References

1 MEI, K.K., POUS, R., CHEN, Z., LIU, Y.W., and PROUTY, M.D.: 'The measured equation of invariance: A new concept in field computations', *IEEE Trans. Antennas Propag.*, 1994, **42**, (3)

2 JETVIC, J.O., and LEE, R.: 'A theoretical and numerical analysis of the measured equation of invariance', *IEEE Trans. Antennas Propag.*, 1994, **42**, (8), pp. 1097–1105

3 RIUS, J.M., PARRON, J., POUS, R., and CADAMA, A.: 'The measured equation of invariance: A proof for the postulates and a new formulation as a sparse matrix integral equation method'. 1994 URSI Radio Science Meeting, Seattle, Washington, 19–24 June 1994

4 HARRINGTON, R.F.: 'Time-harmonic electromagnetic fields' (McGraw-Hill, 1961)

Current mode filter structure based on dual output transconductance ampifiers

B. Al-Hashimi

Indexing terms: Current-mode circuits, Active filters

A new current-mode filter structure based on the dual output operational transconductance amplifier is described. By appropriate choice of components, the structure provides lowpass, highpass and bandpass responses. Experimental results which confirm the theoretical analysis are given.

Introduction: In recent years there has been considerable interest in two particular developments in active filter design. First, the use of current mode devices in filter configurations, examples include current conveyors [1, 2], operational transconductance amplifiers [3, 4] and current feedback amplifier [5, 6] based filters. Secondly, the realisation of current rather than voltage-based network functions [7]. These developments bring the benefits of simple, low sensitivity filter configurations which may be implemented at high frequencies. In the case of operational transconductance amplifier (OTA) based filters, two types of amplifier have been used: single output OTAs and dual output OTAs. It has been shown that dual output OTA based filters perform better than the single output OTAs [8–10], in particular in higher frequency of operation. Also, dual output operational transconductance amplifiers (DO-OTAs) usually simplify the development of current transfer functions owing to the multiple current outputs. In this Letter, a new current-mode filter structure based on the DO-OTA is described.

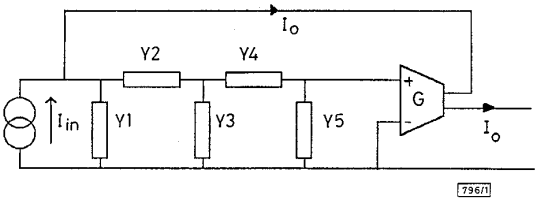

Fig. 1 *General filter structure*

General filter structure description: The proposed general filter structure is shown in Fig. 1. The current transfer function of the circuit is

$$\frac{I_o}{I_{in}} = \frac{Y2Y4G}{Y1Y4(Y2+Y3+Y5)+Y2Y4(Y3+Y5+G)Y1Y5(Y2+Y3)+Y2Y3Y5} \quad (1)$$

where G denotes the transconductance of the amplifier and $Y1$ to $Y5$ are the admittances. The dual output of the OTA is used for performing two functions. One of the outputs provides the feedback required for providing the complex poles, while the other output is used to provide pure current output which can be used as input to similar sections in cascade configurations. Specific second-order lowpass, highpass, and bandpass filters are obtained through suitable selection of the admittances as shown in Table 1.

Table 1: Specification of general filter structure components

	$Y1$	$Y2$	$Y3$	$Y4$	$Y5$
Lowpass	$sC1$	$g1$	$sC2$	∞	0
Highpass	$g1$	$sC1$	$g2$	$sC2$	$g3$
Bandpass	$g1$	$g2$	$sC1$	$sC2$	$g3$

(i) *Lowpass filter:* A lowpass filter is obtained by substituting the admittances specified in the 1st row of Table 1 in eqn. 1

$$\frac{I_o}{I_{in}} = \frac{g1G}{C1C2s^2 + g1(C1 + C2)s + g1G}$$

Assuming $C1 = C2 = 1$F and comparing with the standard form of the second-order filter transfer function, leads to the following simple design equations

$$g1 = \frac{\omega_0}{2Q} \qquad G = 2Q\omega_0$$

(ii) *Highpass filter:* Substituting the admittances specified in the 2nd row of Table 1 into eqn. 1, and letting $C1 = C2 = 1$ F and $g1 = g2 = g3 = g$, a highpass filter is obtained as shown

$$\frac{I_o}{I_{in}} = \frac{Gs^2}{(3g + G)s^2 + (4g^2)s + g^3}$$

This filter has the following design equations:

$$g = 4Q\omega_0 \qquad G = 4Q\omega_0(16Q^2 - 3)$$

(iii) *Bandpass filter:* Substituting the admittances specified in the last row of Table 1 into eqn. 1 and using $C1 = C2 = 1$F and $g1 = g2 = g3 = g$, a bandpass filter is obtained as shown

$$\frac{I_o}{I_{in}} = \frac{Gs}{2s^2 + (5g + G)s + g^2}$$

This filter has the following design equations:

$$g = \sqrt{2} * \omega_0 \qquad G = \omega_0\left(5\sqrt{2} - \frac{2}{Q}\right)$$

Experimental results: At the simplest level, the transconductance amplifier of Fig. 1 can be replaced by a single bipolar transistor, since the various filters (lowpass, highpass and bandpass) are obtained using only one of the differential inputs of the transconductance amplifier. The required G of the amplifier is set up by the resistor RE, where $G = 1/(RE+re)$. Using this simplification, and setting up the required currents, the lowpass DO-OTA based filter is shown in Fig. 2. The transistors TR2 and TR3 form a current source to supply the required feedback and output currents, while TR4 and TR5 mirror the current in TR1 to provide an output. To simplify the testing of the filter, it is more convenient to work with voltages than currents and for this reason, transistor TR6 is used. The gain of this circuit is R_L/R_C.

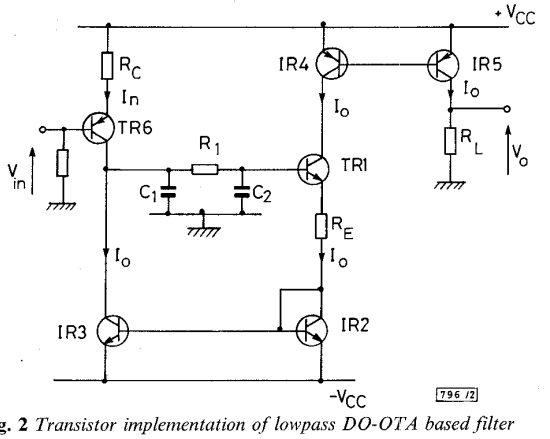

Fig. 2 *Transistor implementation of lowpass DO-OTA based filter*

The circuit of Fig. 2 was constructed using TPQ6502 *npn/pnp* transistor arrays, passive components with 1% tolerances and ±12V supplies, to realise a second order lowpass with $Q = 10$ and $F_0 = 30$kHz. Fig. 3 shows the practical results obtained, in which the measured Q and F_0 were found to be in error by only 1 and 0.5%, respectively. To investigate the high frequency performance of the proposed structure, a Butterworth lowpass filter with a cut-off frequency of 1MHz was implemented. The practical frequency response of the filter is shown in Fig. 4, where the measured cutoff frequency was 0.997MHz. Finally, highpass and bandpass DO-OTA based filters were also built and found to perform well in practice.